

Efficient Near-Infrared Polymer and Organic Light-Emitting Diodes Based on Electrophosphorescence from (Tetraphenyltetranaphtho[2,3]porphyrin)-platinum(II)

Jonathan R. Sommer,[†] Richard T. Farley,[†] Kenneth R. Graham,[†] Yixing Yang,[‡] John R. Reynolds,^{*,†} Jianguo Xue,^{*,†} and Kirk S. Schanze^{*,†}

Department of Chemistry, Center for Macromolecular Science and Engineering, University of Florida, Gainesville, Florida 32611-7200, and Department of Materials Science and Engineering, University of Florida, Gainesville, Florida 32611-6400

ABSTRACT The new metalloporphyrin Pt(tptnp), where tptnp = tetraphenyltetranaphtho[2,3]porphyrin, has been prepared and subjected to photophysical and electrooptical device studies. In degassed toluene solution at room temperature Pt(tptnp) features efficient phosphorescence emission with λ_{max} 883 nm with a quantum efficiency of 0.22. The complex has been used as the active phosphor in polymer and organic light-emitting diodes. Polymer light-emitting diodes based on a spin-coated emissive layer consisting of a blend of Pt(tptnp) doped in poly(9-vinylcarbazole) and 2-(4-biphenyl)-5-(4-*tert*-butylphenyl)-1,3,4-oxadiazole exhibit near-IR emission with λ_{max} 896 nm, with a maximum external quantum efficiency (EQE) of 0.4% and a maximum radiant emittance of 100 $\mu\text{W}/\text{cm}^2$. Organic light-emitting diodes prepared via vapor deposition of all layers and that feature an optimized multilayer hole injection and electron blocking layer heterostructure with an emissive layer consisting of 4,4'-bis(carbazol-9-yl)biphenyl (CBP) doped with Pt(tptnp) exhibit a maximum EQE of 3.8% and a maximum radiant emittance of 1.8 mW/cm^2 . The polymer and organic light-emitting diodes characterized in this study exhibit record high efficiency for devices that emit in the near-IR at $\lambda > 800$ nm.

KEYWORDS: polymer light emitting diodes • organic light emitting diodes • near-infrared • electrophosphorescence • metalloporphyrin

INTRODUCTION

Near-infrared (near-IR) polymer and organic light-emitting devices (PLED and OLED, respectively) are of interest due to their possible applications in a number of areas, including infrared signaling and displays, telecommunications, and wound healing (1–4). The most common approach that has been taken to develop near-IR emitting devices is to employ metal-organic complexes that feature lanthanides (Yb, Nd, Er, etc.) as the near-IR light-emitting centers (5–10). Lanthanide-containing materials have the advantage of giving rise to narrow-bandwidth emission at a number of specific wavelengths across the near-IR band (800–1600 nm), depending upon the specific lanthanide used. However, due to the low intrinsic photoluminescence (PL) quantum efficiency of the metal-centered F states, light-emitting devices based on lanthanide complexes suffer from low overall quantum efficiency, with

record quantum yields in the 0.1–0.5% range (5–10). We recently reported near-IR emitting OLEDs based on low-bandgap, fluorescent conjugated oligomers that operate with external quantum efficiencies (EQE) up to 1.6% (11). However, while these systems are clearly of interest, their emission is relatively broad, and the quantum efficiency of devices based on materials that emit beyond 1000 nm is low (12).

High-efficiency, visible electrophosphorescent devices have been fabricated on the basis of metal-organic and organometallic complexes that display efficient phosphorescence. One of the first examples demonstrating the concept of using phosphorescent emitters in LEDs was based on Pt(oep) (oep = octaethylporphyrin) (13). When this complex is incorporated into an optimized multilayer OLED, the device gives rise to efficient red electroluminescence at 650 nm with an EQE of $\sim 4\%$. Recently, Thompson and co-workers have extended the concept of using phosphorescent metalloporphyrin emitters in the near-IR by using Pt(tptbp) (tptbp = tetraphenyltetraenzoporphyrin) to develop a high-efficiency OLED that emits at 772 nm with an EQE of $\sim 6.3\%$ (14, 15). This work demonstrates the feasibility of making high-efficiency, near-IR electrophosphorescent OLEDs; however, additional work is needed to extend the emission wavelength further into the near-IR spectral region.

* To whom correspondence should be addressed. E-mail: reynolds@chem.ufl.edu (J.R.R.); jxue@mse.ufl.edu (J.X.); kschanze@chem.ufl.edu (K.S.S.).

Received for review December 12, 2008 and accepted January 15, 2009

[†] Department of Chemistry, Center for Macromolecular Science and Engineering.

[‡] Department of Materials Science and Engineering.

DOI: 10.1021/am800236x

© 2009 American Chemical Society

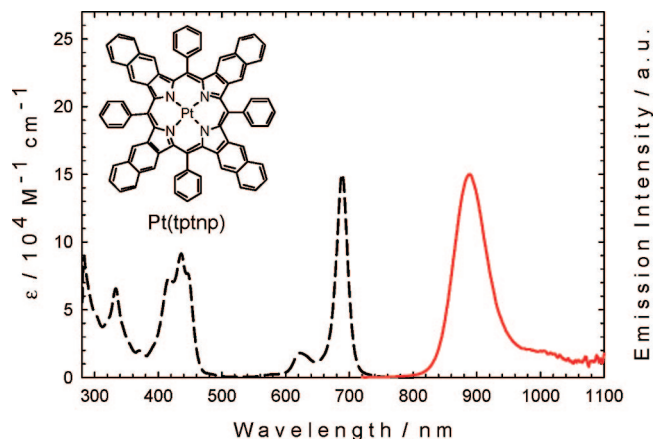


FIGURE 1. Absorption (black dashed line) and photoluminescence (red solid line) of Pt(tptnp) in toluene. The molecular structure is shown in the inset.

Herein, we report the fabrication of high-efficiency PLED and OLED devices that emit in the near-IR at ~ 900 nm. These devices feature emissive layers (EMLs) that contain Pt(tptnp) (tptnp = tetraphenyltetranaphtho[2,3]porphyrin) as the phosphor (see Figure 1 inset for chemical structure). The near-IR emitting devices described in this report are the highest efficiency reported to date for emissions at wavelengths beyond 800 nm. In particular, a solution-processed PLED that features Pt(tptnp) in a blend of poly(9-vinylcarbazole) (PVK) and (2-(4-biphenyl)-5-(4-*tert*-butylphenyl)-1,3,4-oxadiazole) (PBD) exhibits a maximum EQE of $\sim 0.4\%$, with a maximum radiant emittance of $100 \mu\text{W}/\text{cm}^2$. Further, an optimized multilayer vapor deposited OLED that contains an emissive layer consisting of a host of 4,4'-bis(carbazol-9-yl)biphenyl (CBP) doped with Pt(tptnp) exhibits a maximum EQE of $\sim 3.8\%$ and a maximum radiant emittance of $1.8 \text{ mW}/\text{cm}^2$.

RESULTS AND DISCUSSION

The complex that is the basis of this work, Pt(tptnp), was prepared for the first time by metalation of the free base tptnp, which was prepared in several synthetic steps according to a literature procedure (16, 17). Metalation was carried out by treating tptnp with platinum(II) acetate in refluxing benzonitrile solution. The reaction was monitored using absorption spectroscopy, as the Q band, which appears at λ_{max} 724 nm for tptnp, blue-shifts to 689 nm for the Pt(II) complex. After purification, the structure of Pt(tptnp) was confirmed by ^1H and ^{13}C NMR and high-resolution mass spectroscopy.

The absorption and PL spectra of Pt(tptnp) in toluene are shown in Figure 1. The complex exhibits Soret absorption at λ_{max} 436 nm and a single Q band at 689 nm. In argon-degassed toluene solution, the PL of the complex is dominated by a single phosphorescence band with λ_{max} 883 nm and a weak vibronic shoulder at $\lambda \sim 1000$ nm. The phosphorescence quantum yield for Pt(tptnp) is $\phi_p = 0.22$ in toluene, and the triplet-state lifetime was determined by transient absorption spectroscopy (see Figure S1 in the Supporting Information) to be $\tau = 8.5 \mu\text{s}$. The phosphores-

cence yield and lifetime of Pt(tptnp) are less than that of Pt(tptbp), which are reported to be $\phi_p = 0.7$ and $\tau = 53 \mu\text{s}$, respectively (15). The lower ϕ_p and τ values for Pt(tptnp) compared to those for Pt(tptbp) are in accord with the energy gap law, which indicates that the rate of nonradiative decay increases with decreasing (triplet) excited-state energy (18, 19). Despite the fact that the phosphorescence quantum yield is lower for the near-IR-emitting porphyrin, this room-temperature phosphorescence yield is the highest that has ever been reported for a compound that emits beyond 800 nm, making the phosphor an excellent choice for incorporation into near-IR light-emitting devices.

Thin films with varying concentrations of Pt(tptnp) blended into a PVK:PBD (60:40) host were deposited by spin coating on glass substrates which had been coated with a layer of the conducting polymer poly(3,4-ethylenedioxythiophene):poly(styrenesulfonate) (PEDOT:PSS), and photoluminescence (PL) measurements were carried out to study energy transfer from the host to the Pt(tptnp) dopant. At low dopant concentration (< 2 wt % Pt(tptnp)), the PL of the films is dominated by the fluorescence from the PVK:PBD host, with strong emission observed with $\lambda_{\text{max}} \sim 430$ nm (excitation at 345 nm). As the Pt(tptnp) concentration in the blend is increased, the host fluorescence is quenched, and although phosphorescence from Pt(tptnp) is observed at 886 nm, the intensity does not increase substantially. For a blend containing 8 wt % of Pt(tptnp) the fluorescence from the host is still observed with approximately 15% intensity relative to the phosphorescence from the Pt(tptnp) dopant. These experiments illustrate that the host is able to sensitize PL from the Pt(tptnp) dopant, presumably via dipole–dipole energy transfer. However, the quenching of the host fluorescence is incomplete even when Pt(tptnp) is present at 8 wt %, suggesting that there may be some degree of aggregation of the Pt(tptnp) dopant creating PVK:PBD rich regions wherein energy transfer is inefficient.

PLEDs with the structure glass/ITO/PEDOT:PSS/Pt(tptnp):PVK:PBD/LiF/Ca/Al were fabricated by spin-coating the active layer on top of a PEDOT:PSS layer, followed by evaporation of the metal electrode materials. Light emission from the PLEDs turns on at an applied voltage of ~ 6 V, and for blends containing Pt(tptnp) at ≥ 2 wt % the emission is observed exclusively in the near-IR (Figure 2) at λ_{max} 896 nm. This result suggests that emission from the dopant is obtained through a charge-trapping mechanism, as opposed to the dipole–dipole energy transfer as observed in the thin film PL. In particular, it is likely that holes are selectively trapped on the Pt(tptnp) dopant, and consequently charge carrier recombination occurs selectively on the phosphor, producing near-IR emission. Devices that contain PVK:PBD blends with 4 wt % Pt(tptnp) display the highest external quantum efficiencies with solely Pt(tptnp) emission. Figure 3 shows the radiant emittance–current density–voltage ($R-J-V$) characteristics and the current density dependence of the external quantum and power efficiencies of two optimized near-IR emitting PLEDs having active layers of thickness 85 and 130 nm. Both sets exhibit maximum

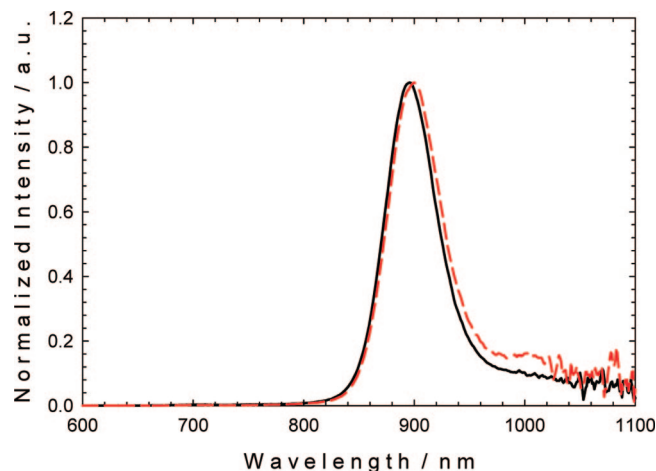


FIGURE 2. Electroluminescence spectra for 85 nm active layer PLED (black solid line) and an OLED with a nominally undoped electron transport layer (red dashed line). The drive voltage is 20 V for PLED and 6 V for OLED (corresponding to a current density of 1 mA/cm²).

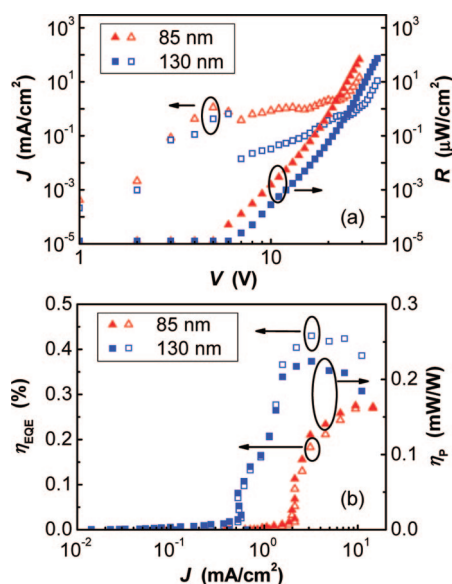


FIGURE 3. Device characteristics for PLEDs: (a) current density, J , and the radiant emittance in the forward viewing directions, R , as functions of the voltage, V , for emissive layers of 85 nm (triangles) and 130 nm thickness (squares); (b) external quantum efficiency, η_{EQE} , and power efficiency, η_p , of these two devices as functions of J .

radiant emittance of approximately 100 $\mu\text{W}/\text{cm}^2$; however, the device with the thicker emitting layer features noticeably higher external quantum efficiency (0.4%) and power efficiency (0.22 mW/W). The devices operate at relatively high voltages due to the thickness of the emissive layer and the high electron and hole injection barriers at the electrodes.

OLEDs based on the Pt(tpnp) phosphor were fabricated via vacuum thermal evaporation. The emissive layer (EML), consisting of CBP doped with 8 wt % Pt(tpnp), was sandwiched between a hole transport layer (HTL) of bis[*N*-(1-naphthyl)-*N*-phenylamino]biphenyl (α -NPD) and an electron transport layer (ETL) of 4,7-diphenyl-1,10-phenanthroline (BPhen). In one device (specified as the “undoped device”), the entire 100 nm ETL layer is nominally undoped. In another device (specified as the “*n*-doped device”), Cs was

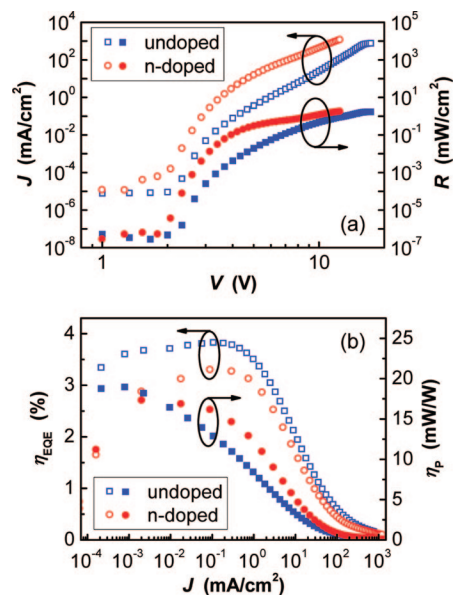


FIGURE 4. Device characteristics for OLEDs: (a) current density, J , and the radiant emittance in the forward viewing directions, R , as functions of the voltage, V , for the undoped and *n*-doped devices; (b) external quantum efficiency, η_{EQE} , and power efficiency, η_p , of these two devices as functions of J .

used to *n*-dope BPhen (BPhen:Cs = 1:0.2, molar ratio) except in the 15 nm layer adjacent to the EML. Cs has been shown to serve as an effective *n*-type dopant in BPhen to increase the conductivity of the ETL and improve the efficiency of electron injection from the cathode (20).

Light emission from the vacuum-deposited Pt(tpnp)-based OLEDs turns on at low voltage (~ 2 V), and the emission occurs exclusively in the near-IR at 900 nm (Figure 2). The R - J - V characteristics of the doped and undoped OLEDs are compared in Figure 4a. At $V > 2.5$ V, the current density was approximately 2 orders of magnitude higher in the *n*-doped device, due to the significantly enhanced conductivity in the *n*-doped ETL compared with that in the nominally undoped ETL (20). The undoped device features a turn-on voltage of approximately 2.2 V, even though the BPhen ETL is rather thick (100 nm), while the turn-on voltage is further reduced to 2.0 V for the *n*-doped device. Maximum radiant emittances of $R \approx 1.8$ mW/cm² are obtained (at $V = 17$ V in the undoped device and $V = 12$ V in the *n*-doped device), which are similar to those obtained from our previously reported fluorescent near-IR OLEDs that emit at shorter wavelengths (peak emission at 700–815 nm) (11). Figure 4b shows the current density dependencies of the EQE and power efficiencies of these two OLEDs. For the undoped device, the EQE is relatively constant at low current densities and reaches a maximum of $\eta_{\text{EQE}} = 3.8 \pm 0.3\%$ at $J \approx 0.1$ mA/cm²; however, at $J > 1$ mA/cm², it decreases significantly with the increase of the current density to $\eta_{\text{EQE}} = 2.0\%$ at $J = 10$ mA/cm² and $\eta_{\text{EQE}} = 0.6\%$ at $J = 100$ mA/cm². The significant rolloff in efficiency at higher current densities is likely due to the triplet-triplet exciton annihilation process that commonly occurs in phosphorescent OLEDs (21). The maximum power efficiency of the undoped device is $\eta_p = 19 \pm 3$ mW/W, achieved at low current densities ($J \approx 10^{-3}$ mA/cm²). Such efficiency is approxi-

mately 3–10 times higher than the maximum η_p of the near-IR fluorescent OLEDs we reported earlier (11). In comparison with the undoped device, the *n*-doped device has slightly lower quantum efficiencies with a maximum of $\eta_{\text{EQE}} = 3.3\%$. The maximum η_p value of the *n*-doped device is $\eta_p = 17$ mW/W, also slightly lower than for the undoped device; however, the lower drive voltage resulting from the increased conductivity of the *n*-doped ETL leads to higher power efficiencies at $J > 10^{-2}$ mA/cm² for the *n*-doped device. For example, at $J = 1$ mA/cm², $\eta_p = 12$ mW/W for the *n*-doped device, which is more than 40% higher than that of the undoped device (8.4 mW/W).

The efficiencies of the vacuum-deposited OLED devices are significantly higher than those of the solution-processed PLED devices. These higher efficiencies can be attributed to the multilayer structure of the OLED devices, which helps to confine charge carriers to the emissive layer as well as to minimize aggregation quenching effects occurring in the PLEDs. Preliminary atomic force microscopy and transmission electron microscopy studies of the Pt(tptnp)-doped PVK:PBD films confirms the presence of aggregates. A systematic study of the effect of concentration and porphyrin structure is the subject of ongoing work and will be reported in a forthcoming full paper.

In summary, we report the synthesis and photophysical characterization of Pt(tptnp), which emits phosphorescence at 883 nm with a quantum yield in solution of 0.22. This is the most efficient phosphorescent emitter that has ever been reported that emits at $\lambda > 800$ nm. By using Pt(tptnp) as the phosphor, we have fabricated near-IR polymer and organic light-emitting devices that display electrophosphorescence at $\lambda \sim 900$ nm, with a bandwidth of ~ 100 nm. The PLEDs and OLEDs exhibit record high-efficiency electrophosphorescence for devices that emit at $\lambda > 800$ nm.

EXPERIMENTAL SECTION

Synthesis of Platinum Tetraphenyltetranaphtho[2,3]-porphyrin. The starting materials platinum(II) acetate and tetraphenyltetranaphtho[2,3]porphyrin (tptnp) were synthesized as previously reported in the literature (16, 17, 22). A 50 mL Schlenk flask was charged with 0.112 g of tptnp and 0.150 g of platinum(II) acetate dissolved in 25 mL of benzonitrile. The solution was deoxygenated with argon for 45 min prior to heating. The reaction mixture was kept under an argon atmosphere and refluxed in an oil bath at 190 °C for 12 h. The reaction mixture was cooled to room temperature and the solvent removed by vacuum distillation. The crude material was passed through a 4 in. length \times 2 in. diameter column of neutral silica with a dichloromethane/tetrahydrofuran solvent mixture (9:1 v:v) as eluent. The first dark green band was collected, and the solvent was evaporated under reduced pressure. The product was further purified by reprecipitation by dissolution in warm dichloromethane followed by dropwise addition to excess acetonitrile and storage overnight in a refrigerator. The precipitate was collected on a fine fritted funnel and washed repeatedly with cold methanol, affording 70 mg of Pt(tptnp) as a dark green powder; yield 53%.

Spectral Data. The ¹H and gHMBC spectra of compound Pt(tptnp) were taken on a Varian Inova 500 NMR spectrometer, equipped with a 5 mm indirect detection probe and z-axis gradients and operating at 500 MHz for ¹H and 125 MHz for ¹³C. The chemical shifts were referenced to the residual solvent

signals: 7.22 ppm in ¹H and 123.9 in ¹³C. Because of the limited solubility of Pt(tptnp) in the NMR solvent, ¹³C chemical shifts were measured by indirect detection, in a gHMBC spectrum. ¹H NMR (pyridine-*d*₅): δ 8.47–8.44 (m, 8H), 8.22–8.14 (m, 4H), 8.10–8.05 (m, 8H), 7.93 (s, 8H), 7.90–7.84 (m, 8H), 7.61 (8H, overlap with solvent). ¹³C NMR (pyridine-*d*₅): δ 142.4, 135.9, 134.2, 131.6, 130.5, 130.0, 129.7, 126.7, 124.1, 117.9. ESI-TOF *m/z* 1206.3188, calcd 1206.3157.

Optical Characterization. Absorption spectra were measured using a PerkinElmer Lambda 25 UV–vis spectrometer. The PL spectra were obtained by excitation at the Soret band absorption maximum and recorded with an ISA SPEX Triax 180 spectrograph coupled to a Spectrum-1 liquid nitrogen cooled silicon charge coupled device detector. This spectrometer has a relatively flat spectral response to 900 nm, although there is some loss in efficiency due to the grating, which is blazed in the visible region. The solution phosphorescence quantum yield was calculated relative to ZnTPP in CH₂Cl₂ ($\phi = 0.033$) (23) according to a previously described method (24). The sample and actinometer solutions had matched optical density at the excitation wavelength, and the emission spectra were corrected for the spectrometer response prior to being used to compute the quantum yield. Time-resolved transient absorption spectra of Pt(tptnp) in toluene were collected by using previously described laser systems for the visible and near-IR regions (25). PL measurements of Pt(tptnp):PVK:PBD blends spin-coated from chlorobenzene solution were performed on the apparatus described above, and samples were excited at 345 nm to maximize host polymer absorption.

Device Fabrication and Characterization. PLEDs were fabricated on prepatterned indium tin oxide (ITO) coated glass substrates with a sheet resistance of ~ 20 Ω/\square . The ITO substrates were cleaned sequentially with a sodium dodecyl sulfate solution, acetone, and isopropyl alcohol followed by exposure to an oxygen plasma. A layer of PEDOT:PSS (Baytron P VP Al4083) was spin-coated on the ITO immediately following oxygen plasma exposure and then annealed at 120 °C under vacuum for 2 h. The active layer solutions consisting of varying weight percentages of Pt(tptnp) in PVK:PBD (60:40) were prepared and spin-coated from chlorobenzene in an MBraun glovebox with < 0.1 ppm oxygen and water. The cathode consisting of LiF (1 nm), Ca (10 nm), and Al (80 nm) was deposited in a thermal evaporator under a vacuum of 10^{-6} Torr. Radiant emittance (*R*)–voltage (*V*) measurements were carried out using a calibrated UDT Instruments silicon detector. Current density (*J*)–voltage (*V*) measurements were made using a Keithley 2400 sourcemeter. The electroluminescence (EL) spectra were collected using the ISA SPEX Triax 180 spectrograph with the device driven using the Keithley sourcemeter. Each 2.5 \times 2.5 cm substrate features eight independently addressable pixels with area 0.07 cm², and the results presented in Figure 3 represent measurements averaged over three pixels.

The near-IR OLEDs were fabricated on glass substrates commercially coated with an ITO anode with a sheet resistance of ~ 20 Ω/\square . The substrates were cleaned in ultrasonic baths of deionized water, acetone, and isopropyl alcohol consecutively for 15 min each and then exposed to an ultraviolet ozone environment for 15 min immediately before loading into a high-vacuum chamber (base pressure $\sim 10^{-7}$ Torr). All the layers, including the cathode, were deposited using vacuum thermal evaporation following procedures published previously (26). The thicknesses of the HTL and EML were 40 and 20 nm, respectively, whereas the ETL layer thickness was 100 nm, optimized to achieve the highest device efficiencies. A 1 nm layer of LiF followed by a 100 nm Al layer was then deposited as the cathode. Radiant emittance (*R*)–current density (*J*)–voltage (*V*) characteristics were measured under ambient conditions using an Agilent 4155C semiconductor parameter analyzer and a calibrated Newport silicon detector. The EL spectra were col-

lected as described above, with the devices driven at a constant current. The radiant emittance for both OLEDs and PLEDs was calibrated assuming Lambertian emission, and the EQE (η_{EQE}) and electrical-to-optical power efficiency values (η_p) were derived on the basis of the recommended methods (27). Each 2.5×2.5 cm substrate features four independently addressable pixels with area 4 mm^2 , and the results presented in Figure 4 represent measurements averaged over at least eight pixels.

Acknowledgment. We gratefully acknowledge financial support from the U.S. Defense Advanced Research Projects Agency (DARPA) and the U.S. Army Aviation and Missile Research, Development, and Engineering Center (AMRDEC) (Project No. W31P4Q-08-1-0003) (28).

Supporting Information Available: A figure giving transient absorption difference spectra of Pt(tpntp). This material is available free of charge via the Internet at <http://pubs.acs.org>.

REFERENCES AND NOTES

- Whelan, H. T.; Smits, R. L.; Buchman, E. V.; Whelan, N. T.; Turner, S. G.; Margolis, D. A.; Cevenini, V.; Stinson, H.; Ignatius, R.; Martin, T.; Cwiklinski, J.; Philippi, A. F.; Graf, W. R.; Hodgson, B.; Gould, L.; Kane, M.; Chen, G.; Caviness, J. J. *Clin. Laser Med. Surg.* **2001**, *19*, 305–314.
- Karu, T. *The Science of Low-Power Laser Therapy*; Gordon and Breach Scientific: New York, 1998.
- Raghavachari, R. *Near-Infrared Applications in Biotechnology*; CRC Press: Boca Raton, FL, 2001.
- Desurvire, E. *Erbium-Doped Fiber Amplifiers: Principles and Applications*; Wiley-Interscience: New York, 1994.
- Sun, R. G.; Wang, Y. Z.; Zheng, Q. B.; Zhang, H. J.; Epstein, A. J. *J. Appl. Phys.* **2000**, *87*, 7589–7591.
- Kawamura, Y.; Wada, Y.; Yanagida, S. *Jpn. J. Appl. Phys., Part 1* **2001**, *40*, 350–356.
- Harrison, B. S.; Foley, T. J.; Bouguettaya, M.; Boncella, J. M.; Reynolds, J. R.; Schanze, K. S.; Shim, J.; Holloway, P. H.; Padmanaban, G.; Ramakrishnan, S. *Appl. Phys. Lett.* **2001**, *79*, 3770–3772.
- Slooff, L. H.; Polman, A.; Cacialli, F.; Friend, R. H.; Hebbink, G. A.; van Veggel, F.; Reinhoudt, D. N. *Appl. Phys. Lett.* **2001**, *78*, 2122–2124.
- Harrison, B. S.; Foley, T. J.; Knefely, A. S.; Mwaura, J. K.; Cunningham, G. B.; Kang, T. S.; Bouguettaya, M.; Boncella, J. M.; Reynolds, J. R.; Schanze, K. S. *Chem. Mater.* **2004**, *16*, 2938–2947.
- de Bettencourt-Dias, A. *Dalton Trans.* **2007**, 2229–2241.
- Yang, Y.; Farley, R. T.; Steckler, T. T.; Eom, S.-H.; Reynolds, J. R.; Schanze, K. S.; Xue, J. *Appl. Phys. Lett.* **2008**, *93*, 163305.
- Qian, G.; Zhong, Z.; Luo, M.; Yu, D.; Zhang, Z.; Wang, Z. Y.; Ma, D. *Adv. Mater.* **2009**, *21*, 111–116.
- Baldo, M. A.; O'Brien, D. F.; You, Y.; Shoustikov, A.; Sibley, S.; Thompson, M. E.; Forrest, S. R. *Nature* **1998**, *395*, 151–154.
- Sun, Y.; Borek, C.; Hanson, K.; Djurovich, P. I.; Thompson, M. E.; Brooks, J.; Brown, J. J.; Forrest, S. R. *Appl. Phys. Lett.* **2007**, *90*, 5.
- Borek, C.; Hanson, K.; Djurovich, P. I.; Thompson, M. E.; Aznavour, K.; Bau, R.; Sun, Y. R.; Forrest, S. R.; Brooks, J.; Michalski, L.; Brown, J. *Angew. Chem., Int. Ed.* **2007**, *46*, 1109–1112.
- Finikova, O. S.; Cheprakov, A. V.; Vinogradov, S. A. *J. Org. Chem.* **2005**, *70*, 9562–9572.
- Finikova, O. S.; Aleshchenkov, S. E.; Brinas, R. P.; Cheprakov, A. V.; Carroll, P. J.; Vinogradov, S. A. *J. Org. Chem.* **2005**, *70*, 4617–4628.
- Caspar, J. V.; Meyer, T. J. *J. Phys. Chem.* **1983**, *87*, 952–957.
- Wilson, J. S.; Chawdhury, N.; Al-Mandhary, M. R. A.; Younus, M.; Khan, M. S.; Raithby, P. R.; Köhler, A.; Friend, R. H. *J. Am. Chem. Soc.* **2001**, *123*, 9412–9417.
- Walzer, K.; Maennig, B.; Pfeiffer, M.; Leo, K. *Chem. Rev.* **2007**, *107*, 1233–1271.
- Baldo, M. A.; Adachi, C.; Forrest, S. R. *Phys. Rev. B* **2000**, *62*, 10967–10977.
- Basato, M.; Biffis, A.; Martinati, G.; Tubaro, C.; Venzo, A.; Ganis, P.; Benetollo, F. *Inorg. Chim. Acta* **2003**, *355*, 399–403.
- Foley, T. J.; Harrison, B. S.; Knefely, A. S.; Abboud, K. A.; Reynolds, J. R.; Schanze, K. S.; Boncella, J. M. *Inorg. Chem.* **2003**, *42*, 5023–5032.
- Crosby, G. A.; Demas, J. N. *J. Phys. Chem.* **1971**, *75*, 991–1024.
- Wang, Y. S.; Schanze, K. S. *Chem. Phys.* **1993**, *176*, 305–319.
- Zheng, Y.; Eom, S.-H.; Chopra, N.; Lee, J.; So, F.; Xue, J. *Appl. Phys. Lett.* **2008**, *92*, 223–301.
- Forrest, S. R.; Bradley, D. D. C.; Thompson, M. E. *Adv. Mater.* **2003**, *15*, 1043–1048.
- The views and conclusions contained in this document are those of the authors and should not be interpreted as representing the official policies, either expressed or implied, of the Defense Advanced Research Projects Agency; the U.S. Army Aviation and Missile Research, Development, and Engineering Center; or the U.S. Government.

AM800236X